Journal of Molecular Structure 1046 (2013) 92–100

Contents lists available at SciVerse ScienceDirect

Journal of Molecular Structure

journal homepage: www.elsevier.com/locate/molstruc

Quantum mechanical and spectroscopic (FT-IR, FT-Raman, ^{1}H NMR and UV) investigations of 2-(p-nitrobenzyl) benzoxazole

J.B. Bhagyasree [a], Hema Tresa Varghese [b], C. Yohannan Panicker [c,*], Jadu Samuel [a], Christian Van Alsenoy [d], Serap Yilmaz [e], Ilkay Yildiz [e], Esin Aki [e]

[a] Department of Chemistry, Mar Ivanios College, Nalanchira, Trivandrum, Kerala, India
[b] Department of Physics, Fatima Mata National College, Kollam, Kerala, India
[c] Department of Physics, TKM College of Arts and Science, Kollam, Kerala, India
[d] Department of Chemistry, University of Antwerp, B2610, Antwerp, Belgium
[e] Faculty of Pharmacy, Department of Pharmaceutical Chemistry, Ankara University, Tandogan, 06100 Ankara, Turkey

HIGHLIGHTS

- IR, Raman spectra and NBO analysis were reported.
- The wavenumbers are calculated theoretically using Gaussian09 software.
- The wavenumbers are assigned using PED analysis.
- NBO, HOMO–LUMO analysis shows ICT, π delocalization in the molecule.

ARTICLE INFO

Article history:
Received 26 December 2012
Received in revised form 9 April 2013
Accepted 9 April 2013
Available online 23 April 2013

Keywords:
FT-IR
FT-Raman
Benzoxazole
Hyperpolarizability
PED

ABSTRACT

The optimized molecular structure, vibrational frequencies, corresponding vibrational assignments of 2-(p-nitrobenzyl)benzoxazole have been investigated experimentally and theoretically using Gaussian09 software package. Potential energy distribution of the normal modes of vibrations are done using GAR2PED program. The optimized geometrical parameters are in agreement with that of similar derivatives. The energy and oscillator strength calculated by Time Dependent Density Functional Theory results almost compliments with experimental findings. Gauge-including atomic orbital ^{1}H NMR chemical shifts calculations were carried out by using B3LYP functional with 6-31G* basis sets. The HOMO and LUMO analysis is used to determine the charge transfer with in the molecule. The stability of the molecule arising from hyper-conjugative interaction and charge delocalization has been analyzed using NBO analysis. MEP was performed by the DFT method and the infrared and Raman intensities have also been reported. Mulliken's net charges have been calculated and compared with the atomic natural charges. The calculated first hyperpolarizability of the title compound is 82.31 time that of the standard NLO material urea and hence is an attractive object for future studies of nonlinear optical properties.

1. Introduction

Benzoxazole derivatives are the structural isoesters of naturally occurring nucleotides such as adenine and guanine, which allows them to interact easily with the biopolymers of living systems and different kinds of biological activity have been obtained [1–5]. It has been reported that they have shown low toxicity in warm-blooded animals [4,6]. Yalcin et al. [7–10] reported the synthesis and microbiological activity of 5-substituted-2-(p-substituted phenyl)benzoxazole derivatives. Anto et al. [11] reported the vibrational spectroscopic and ab initio calculations of 5-methyl-2-(p-fluorophenyl)benzoxazole. Vibrational spectroscopic studies and ab initio calculations of 5-methyl-2-(p-methylaminophenyl)benzoxazole is also reported by Ambujakshan et al. [12]. Ab initio quantum mechanical method is at present widely used for simulating IR spectrum. Such simulations are indispensable tools to perform normal coordinate analysis so that modern vibrational spectroscopy is unimaginable without involving them and time-dependent DFT (TD-DFT) calculations have also been used for the analysis of the electronic spectrum and spectroscopic properties. The energies, degrees of hybridization, populations of the lone electron pairs of oxygen, energies of their interaction with the anti bonding π^* orbitals of the benzene ring, electron density (ED) distributions and $E(2)$ energies have been calculated by NBO analysis using DFT method to give clear evidence of stabilization

* Corresponding author. Tel.: +91 9895370968.
E-mail address: cyphyp@rediffmail.com (C. Yohannan Panicker).

0022-2860/$ - see front matter © 2013 Elsevier B.V. All rights reserved.
http://dx.doi.org/10.1016/j.molstruc.2013.04.044

originating from the hyper conjugation of various intra-molecular interactions. In this work, IR, Raman spectra, ^{1}H NMR parameters and UV–vis spectrum of 2-(p-nitrobenzyl) benzoxazole are described both experimentally and theoretically. The HOMO and LUMO analysis have been used to elucidate information regarding charge transfer within the molecule. There has been growing interest in using organic materials for nonlinear optical (NLO) devices, functioning as second harmonic generators, frequency converters, electro-optical modulators, etc. because of the large second order electric susceptibilities of organic materials. Since the second order electric susceptibility is related to first hyperpolarizability, the search for organic chromophores with large first hyperpolarizability is fully justified. The organic compounds showing high hyperpolarizability are those containing an electron donating group or an electron withdrawing group interacting through a system of conjugated double bonds. In this case, the electron withdrawing group NO_2 is present in the title compound. 2-(p-nitrobenzyl)benzoxazole derivative was investigated for its inhibitory activity on both eukaryotic DNA Topoisomerase I and II in a cell free system [13]. While the title compound did not show any inhibitory activity for Topoisomerase I, it indicated significant activity as eukaryotic DNA Topoisomerase II inhibitors having IC_{50} value of 17 μM, showing higher potency than the reference drug etoposide.

2. Experimental details

For the synthesis of the benzoxazole derivative, using aqueous mineral acids as the condensation reagent did not provide successful results, because of the oxazole ring which was easily hydrolyzed under these conditions [14]. The title compound, 2-(p-nitrobenzyl)benzoxazole was synthesized (Scheme 1) by heating 0.01 mol o-aminophenol with 0.02 mol p-nitrophenyl acetic acid in 12 g polyphosphoric acid with stirring and reflux. At the end of the reaction period, the residue was poured into ice water and neutralized with excess of 10% NaOH solution, extracted with benzene. The benzene solution was dried over anhydrous sodium sulfate and evaporated under diminish pressure. The residue was boiled with 200 mg charcoal in crystallization solvent and after filtered left to crystallize.

The structure of the title compound was supported by elemental analysis and spectral data.

The FT-IR spectrum (Fig. 1) was recorded using KBr pellets on a DR/Jasco FT-IR 6300 spectrometer. The spectral resolution was 2 cm^{-1}. The FT-Raman spectrum (Fig. 2) was obtained on a Bruker RFS 100/s, Germany. For excitation of the spectrum the emission of Nd:YAG laser was used, excitation wavelength 1064 nm, maximal power 150 mW, measurement on solid sample. The spectral resolution after apodization was 2 cm^{-1}.

The ultraviolet absorption spectra of 2-(p-nitrobenzyl) benzoxazole were examined in the range 200–800 nm using Shimadzu

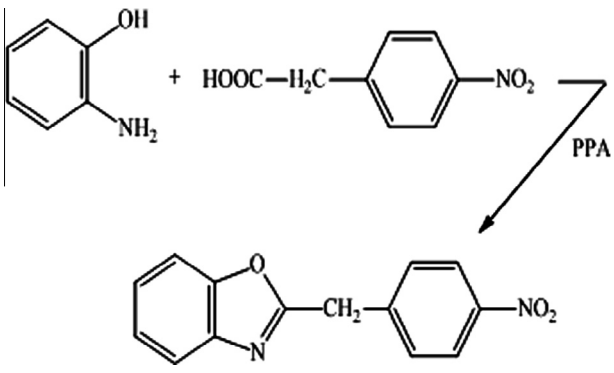

Scheme 1.

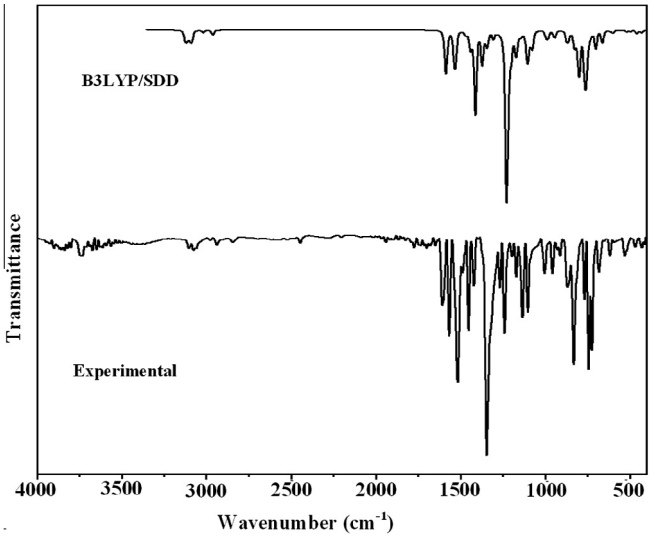

Fig. 1. FT-IR spectrum of 2-(p-nitrobenzyl)benzoxazole.

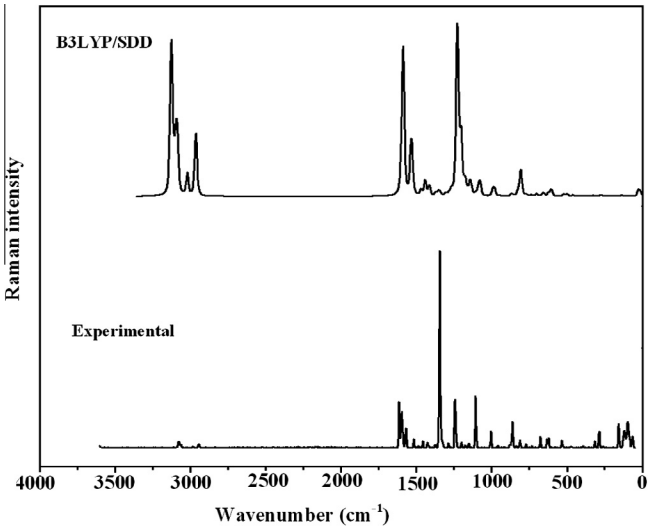

Fig. 2. FT-Raman spectrum of 2-(p-nitrobenzyl)benzoxazole.

UV-2401pc, UV–visible recording spectrometer. The UV pattern is recorded from a 10^{-5} molar solution of title compound dissolved in ethanol (Supporting Information Fig. S1). Chemical Formula:$C_{14}H_{10}N_2O_3$; Molecular Weight: 254.24; *m/z*: 254.07 (100.0%), 255.07 (16.0%), 256.08 (1.1%); Elemental Analysis: Calc./Found: C 66.14, 66.12; H 3.96, 3.957; N 11.02, 11.23; O 18.88, 18.89. ^{1}H NMR spectrum was recorded at 400 MHz on a Varian Inova-400 spectrometer and chemical shifts were reported relative to internal TMS.

3. Computational details

Calculations of the title compound are carried out with Gaussian09 program [15] using the HF/6-31G*, B3LYP/6-31G* and B3LYP/SDD basis sets to predict the molecular structure and vibrational wavenumbers. Molecular geometry was fully optimized by Berny's optimization algorithm using redundant internal coordinates. Harmonic vibrational wavenumbers are calculated using the analytic second derivatives to confirm the convergence to minima on the potential surface. The wavenumber values computed at the Hartree–Fock level contain known systematic errors due to the negligence of electron correlation [16]. We therefore, have used the

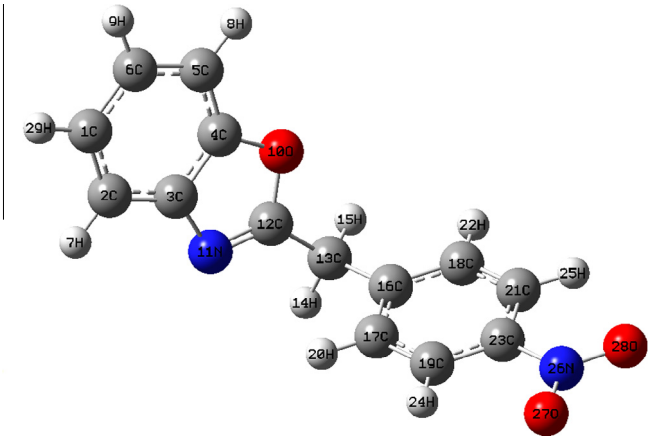

Fig. 3. Optimized geometry (B3LYP/SDD) of 2-(p-nitrobenzyl)benzoxazole.

scaling factor value of 0.8929 for HF/6-31G* basis set. The DFT hybrid B3LYP functional and SDD methods tend to overestimate the fundamental modes; therefore scaling factor of 0.9613 has to be used for obtaining a considerably better agreement with experimental data [16]. The Stuttagard/Dresden effective core potential basis set (SDD) [17] was chosen particularly because of its advantage of doing faster calculations with relatively better accuracy and structures [18]. Then frequency calculations were employed to confirm the structure as minimum points in energy. Parameters corresponding to optimized geometry (SDD) of the title compound (Fig. 3) are given as supporting material (Table S1). The absence of imaginary wavenumbers on the calculated vibrational spectrum in firms that the structure deduced corresponds to minimum energy. In total there are 81 vibrations from 3131 to 14 cm^{-1}. The assignments of the calculated wave numbers are aided by the animation option of GAUSSVIEW program, which gives a visual presentation of the vibrational modes [19]. The potential energy distribution (PED) is calculated with the help of GAR2PED software package [20]. The ^1H NMR data were obtained from the DFT method using basis set 6-31G*. The characterization of excited states and electronic transitions were performed using the time-dependent DFT method (TDB3LYP) on their correspondingly optimized ground state geometries. We used the time-dependent density functional theory (TD-DFT), which is found to be an accurate method for evaluating the low-lying excited states of molecules and has been thoroughly applied to solve physical and chemical problems. Vertical excitation energies were computed for the first 30 singlet excited states, in order to reproduce the experimental electronic spectra. Potential energy surface scan studies have been carried out to understand the stability of planar and non-planar structures of the molecule. The HOMO and LUMO energy calculated by B3LYP/6-31G* and SDD methods. The first hyperpolarizability (β_0) of this novel molecular system is calculated using SDD method, based on the finite field approach. In the presence of an applied electric field, the energy of a system is a function of the electric field. First hyperpolarizability is a third rank tensor that can be described by a $3 \times 3 \times 3$ matrix. The 27 components of the 3D matrix can be reduced to 10 components due to the Kleinman symmetry [21].

4. Results and discussion

4.1. IR and Raman spectra

The observed IR bands with their relative intensities and calculated wave numbers and assignments are given in Table 1. The most characteristic bands in the spectra of nitro compounds are due to the NO_2 stretching vibrations. In nitro compounds, the asymmetric and symmetric NO_2 stretching vibrations are located in the regions 1661–1499 and 1389–1259 cm^{-1}, respectively [22,23]. Nitrobenzene derivatives display $\upsilon_{as}NO_2$ in the region 1535 ± 30 cm^{-1} and 3-nitropyridines at $1530 \pm$ cm^{-1} [22,24] and substituted nitro benzenes [22,23]. υ_sNO_2 appears strongly at 1345 ± 30 cm^{-1}, in 3-nitropyridine at 1350 ± 20 cm^{-1} and in conjugated nitroalkenes [25] at 1345 ± 15 cm^{-1}. For the title compound, SDD calculations give NO_2 stretching vibrations at 1413 and 1352 cm^{-1}. The NO_2 scissors [22] occur at higher wavenumbers (850 ± 60 cm^{-1}) when conjugated to C—C or aromatic molecules, according to some investigators [26,27] with a contribution of the υCN which is expected near 1120 cm^{-1}. For nitrobenzene, δNO_2 is reported [22] at 852 cm^{-1}, for H_2CCHNO_2 at 890 cm^{-1} and 1,3-dinitrobenzene at 904 and 834 cm^{-1}. For the title compound, the band observed at 812 cm^{-1} in the Raman spectrum and at 809 cm^{-1} (SDD) is assigned as δNO_2 mode. In aromatic compounds, the wagging mode ωNO_2 is assigned at 740 ± 50 cm^{-1} with a moderate to strong intensity, a region in which γCH also is active [22]. ωNO_2 is reported at 701 and 728 cm^{-1} for 1,2-dinitrobenzene and at 710 and 772 cm^{-1} for 1,4-dinitrobenzene [22]. For the title compound, the band at 772 cm^{-1} in the Raman spectrum is assigned as ωNO_2 mode. The SDD calculation gives 770 cm^{-1} as ωNO_2 mode. The rocking mode ρNO_2 is active in the region 540 ± 70 cm^{-1} in aromatic nitro compounds [22]. Varsanyi et al. [28] found 70 ± 20 cm^{-1} and Suryanarayana et al. [29] 65 ± 10 cm^{-1} as the torsion of NO_2 for aromatic compounds. In the present case, the deformation mode of NO_2 is assigned at 498 cm^{-1} by the SDD calculations.

The C=N stretching skeletal bands are observed in the range 1672–1566 cm^{-1} [11,30–32]. Saxena et al. [30] reported a value 1608 cm^{-1} for poly benzodithiazole and Klots and Collier [33] reported a value 1517 cm^{-1} for benzoxazole as υC=N stretching mode. The bands observed at 1518 cm^{-1} in both spectra and 1533 cm^{-1} given by calculation is assigned as υC=N for the title compound. C—N stretching vibrations are observed in the region at 1330–1260 cm^{-1} due to stretching of the phenyl carbon–nitrogen bond [34]. For 2-mercaptobenzoxazole, this mode [35] is reported at 1340 cm^{-1} (Raman) and 1325 cm^{-1} (ab initio calculations). Sandhyarani et al. [36] reported υCN at 1318 cm^{-1} for 2-mercaptobenzothiazole. In the present case, the SDD calculations give 1227 and 1204 cm^{-1} as C—N stretching modes.

The vibrations of the CH_2 group, the asymmetric stretch $\upsilon_{as}CH_2$, symmetric stretch υ_sCH_2, scissoring vibration δCH_2 and wagging vibration ωCH_2 appear in the regions, 3000 ± 50, 2965 ± 30, 1455 ± 55 and 1350 ± 85 cm^{-1}, respectively [22,34]. The SDD calculations give $\upsilon_{as}CH_2$ at 3021 and υ_sCH_2 at 2964 cm^{-1}. Experimentally bands are observed at 2975, 2939 in IR and at 2981, 2941 cm^{-1} in the Raman spectrum as CH_2 stretching modes. A carbonyl, nitrile, or nitro group lowers the wave number of the adjacent CH_2 group [37] to about 1425 cm^{-1}. The scissoring mode of the methylene is assigned at 1441 cm^{-1}. The CH_2 wagging mode is observed at 1287 cm^{-1} in the Raman spectrum and at 1288 cm^{-1} theoretically. The band at 1241 cm^{-1} in the IR, 1244 cm^{-1} in Raman spectrum and at 1241 cm^{-1} by theory is assigned to the twisting mode δCH_2. The rocking mode [22] ρCH_2 is expected in the range 895 ± 85 cm^{-1}. The band at 958 cm^{-1} in the IR spectrum and at 951 cm^{-1} by SDD calculations is assigned as ρCH_2 mode for the title compound.

As expected the asymmetric C—O—C vibration produce strong band at 1268 cm^{-1} in the IR and Raman spectrum with SDD value at 1241 cm^{-1}. The symmetric C—O—C stretching vibration appears at 1075 cm^{-1} by theory. The C—O—C stretching is reported at 1250 and 1073 cm^{-1} for 2-mercaptobenzoxazole [31,35].

The existence of one or more aromatic rings in the structure is normally readily determined from the C—H and C=C—C ring related vibrations. The C—H stretching occurs above 3000 cm^{-1} and

Table 1
IR, Raman bands and calculated (scaled) wavenumbers of 2-(p-nitrobenzyl) benzoxazole and assignments.

HF/6-31G*			B3LYP/6-31G*			B3LYP/SDD			IR	Raman	Assignments[a]
υ(cm^{-1})	IR_I	R_A	υ(cm^{-1})	IR_I	R_A	υ(cm^{-1})	IR_I	R_A	υ(cm^{-1})	υ(cm^{-1})	
3065	2.93	107.68	3136	2.43	116.47	313	3.04	115.87	–	–	υCHII(97)
3065	1.92	24.91	3135	0.56	28.00	3129	0.27	22.37	–	–	υCHII(97)
3049	5.72	172.22	3122	6.66	198.06	3124	10.17	238.92	–	–	υCHI(96)
3042	9.08	84.55	3116	10.21	83.75	3117	10.27	41.16	3103	–	υCHI(99)
3025	16.39	134.36	3098	15.16	154.45	3099	14.74	115.90	–	–	υCHI(99)
3022	6.72	66.44	3092	1.75	55.27	3089	2.41	51.42	–	–	υCHII(94)
3017	4.08	45.86	3089	9.24	68.93	3087	9.08	51.92	3078	3071	υCHII(94)
3009	4.36	60.25	3083	3.52	63.98	3083	3.62	46.8	3057	3061	υCHI(93)
2938	2.33	61.94	3005	3.66	67.83	3021	4.37	54.42	2975	2981	$\upsilon_{as}CH_2$(99)
2888	8.64	114.36	2955	6.70	154.43	2964	9.36	176.33	2939	2941	υ_sCH_2(100)
1632	35.31	24.36	1608	3.16	23.71	1598	2.63	33.52	1608	1615	υPhI(67)
1622	9.68	186.24	1602	4.19	193.38	1589	14.48	265.41	–	1597	υPhI(77)
1614	66.01	116.04	1594	48.85	170.38	1585	50.72	135.39	–	–	υPhII(68)
1606	22.48	0.73	1587	2.72	0.41	1576	3.09	0.56	1568	1568	υPhII(69)
1594	93.94	62.19	1544	73.26	167.49	1533	80.97	179.51	1518	1518	$\upsilon N_{11}C_{12}$(71)
1505	10.43	14.04	1491	9.58	8.69	1468	7.22	15.19	1489	1488	υPhII(62)
1477	6.42	4.72	1473	3.87	6.56	1442	5.58	6.71	1453	1455	υPhI(72)
1461	16.18	26.43	1454	16.38	29.13	1441	19.85	27.59	–	–	δCH_2(91)
1455	51.39	4.15	1439	33.92	13.47	1415	71.43	15.16	1422	1425	υPhI(75)
1448	243.46	0.24	1434	86.41	4.25	1413	49.81	7.01	–	–	$\upsilon_{as}NO_2$(64), υPhII(18)
1396	124.49	0.17	1395	44.72	4.92	1372	54.09	7.45	1392	1375	υNO_2(18), υPhII(73)
1341	8.45	3.67	1354	1.65	10.78	1352	2.43	10.16	–	–	υ_sNO_2(71), υPhI(24)
1326	39.70	52.26	1343	14.18	10.45	1343	26.01	7.19	1346	1345	δCH_2(12), υPhII(63)
1322	302.71	253.40	1324	5.77	1.48	1309	10.98	3.21	–	–	δCHII(52), υPhII(16)
1297	8.14	11.77	1300	3.84	5.82	1288	1.45	2.99	–	1287	δCH_2(46), δCHII(15), υPhII(18)
1296	0.28	7.46	1290	0.39	9.21	1271	1.54	10.85	1268	1268	υPhI(67)
1264	25.21	14.81	1254	9.93	14.32	1241	11.42	13.42	1241	1244	δCH_2(45), υ_{as}COC(47)
1232	74.92	2.79	1240	329.86	413.53	1227	315.81	487.87	–	–	υCN(57), υNO_2(18)
1204	39.64	94.15	1212	33.23	133.97	1204	35.94	142.69	–	–	υPhI(24), υCN(55)
1193	13.07	6.38	1187	27.43	29.88	1181	6.71	18.85	1197	1199	δCHII(57), υPhII(25)
1184	12.86	2.62	1183	9.08	1.87	1170	35.01	22.83	1173	1175	υCC(28), υPhII(16), δCHII(55)
1163	14.03	6.33	1164	1.58	8.67	1149	2.68	7.20	–	1149	δCHI(65), υPhI(25)
1146	1.80	7.84	1155	6.55	44.08	1141	6.64	36.78	1134	–	δCHI(59), δCH_2(20)
1136	23.09	7.42	1120	35.61	9.11	1108	47.11	5.16	1104	1107	δCHI(56), υPhI(15)
1108	9.50	34.25	1108	5.24	2.30	1094	9.99	2.68	–	–	δCHII(60), υPhII(17)
1107	5.05	16.49	1095	18.61	42.83	1081	17.34	45.67	–	–	δCHII(14), υPhII(64)
1098	5.60	9.74	1089	21.46	3.49	1075	14.80	3.26	–	–	δPhI(18), υ_sCOC(58)
1053	0.66	2.74	1014	8.78	2.68	1003	0.09	0.57	1005	1005	δCHI(55), υPhII(32)
1047	0.95	1.47	999	7.20	19.03	996	7.48	5.08	–	–	υPhI(37), δCHII(58)
1044	0.01	0.89	996	1.15	4.76	992	1.18	0.24	–	–	γCHII(72), τPhII(15)
1017	6.61	1.99	983	1.11	0.62	989	0.03	0.24	–	–	γCHII(80), τPhII(12)
1001	5.79	0.23	981	0.01	0.18	985	13.63	28.03	–	961	γCHI(81), τPhI(10)
993	9.88	22.16	947	7.01	2.48	951	4.79	0.56	958	–	δCH_2(58), δPhI(27)
958	6.04	2.20	941	2.76	0.60	941	7.38	0.88	913	919	γCHI(91)
913	15.95	3.44	875	7.23	2.69	871	18.97	4.12	–	880	γCHI(61), δPhI(30)
908	0.24	1.55	869	10.02	4.29	868	0.56	0.46	869	–	γCHII(65), τPhII(19)
902	29.08	2.72	861	0.12	3.55	862	7.64	3.43	–	862	γCHI(86), τPhI(10)
884	0.13	2.05	847	0.61	4.05	854	0.33	0.50	–	–	γCHII(96)
865	10.30	3.18	841	19.56	8.20	828	23.26	8.17	833	833	υO–C(36), δRingIII(17), δCH_2(13), δPhI(12)
832	13.09	34.99	823	3.71	46.40	809	6.13	54.50	–	812	δPhII(35), υPhI(15), δNO_2(40)
820	83.86	6.76	807	92.68	5.54	801	78.35	12.34	–	–	δRingIII(53), υCC(22)
804	16.23	12.10	780	9.42	2.96	770	5.05	3.09	–	772	δNO_2(51), τPhII(15)
788	115.33	1.45	758	81.17	1.73	764	101.43	0.51	768	–	γCHI(66), τPhI(18), τRingIII(10)
775	14.28	3.07	745	0.25	3.72	753	26.91	0.53	744	–	τPhII(44), δNO_2(29)
758	9.70	4.76	742	9.62	2.01	735	8.41	3.68	725	730	τPhI(57), τRingIII(22), γCHI(10)
720	33.73	3.36	700	19.00	4.94	702	24.94	6.16	684	–	τPhII(48), γCN(28)
691	19.64	3.92	668	2.40	5.98	664	16.41	2.82	–	677	δPhII(22), δPhI(21), δRingIII(20)
672	7.13	5.97	665	12.92	3.41	656	2.73	6.30	–	–	τPhII(41), γCN(41)
639	0.94	6.21	637	0.53	6.98	622	0.69	7.96	619	635	δPhII(78)
622	4.70	7.46	617	2.68	8.71	606	1.95	11.54	–	623	δRingIII(40), δPhI(48)
616	3.19	3.15	609	2.07	3.39	599	3.18	4.26	587	–	τRingIII(40), δPhII(32)
583	0.34	0.19	572	0.25	0.16	569	0.55	0.25	–	–	δPhI(60), τRingIII(28)
536	5.93	4.24	530	2.35	4.49	522	3.43	5.96	532	534	δPhI(32), τPhII(23), τRingIII(27)
514	5.11	1.46	510	1.84	4.36	498	2.01	5.02	–	–	δNO_2(69)
472	3.72	2.62	466	2.88	1.53	462	5.16	2.58	470	469	τPhII(42), γCC(17), γCN(21)
460	1.09	1.15	456	0.85	0.49	451	0.56	0.54	–	–	δCC(39), δPhI(37)
446	2.73	0.58	433	1.52	0.62	433	3.84	0.72	430	–	τPhI(58), τRingIII(25)
421	0.05	0.05	415	0.16	0.06	408	0.11	0.04	414	–	τPhII(83)
395	14.04	0.95	394	8.02	1.55	387	8.05	1.84	–	394	τPhI(39), δPhII(33)

(*continued on next page*)

Table 1 (*continued*)

HF/6-31G*			B3LYP/6-31G*			B3LYP/SDD			IR	Raman	Assignments[a]
υ(cm^{-1})	IR_I	R_A	υ(cm^{-1})	IR_I	R_A	υ(cm^{-1})	IR_I	R_A	υ(cm^{-1})	υ(cm^{-1})	
345	2.29	1.84	331	2.25	1.95	327	2.57	1.80	–	314	δCC(56), δCN(25)
305	0.22	2.23	299	0.02	1.53	297	0.23	1.28	–	–	τRingIII(23), δPhII(14), τPhI(14), γRingIII(13)
285	3.57	4.31	278	2.87	3.78	275	2.58	3.13	–	287	γCC(33), γCN(54)
264	0.18	1.04	257	0.29	1.42	252	0.37	1.30	–	262	τPhI(72), τRingII(19)
241	0.13	1.55	237	0.23	1.39	235	0.36	1.26	–	–	δCC(43), δCN(34)
180	4.86	0.77	181	3.24	0.61	177	3.47	0.56	–	–	δCC(40), δCN(35)
138	4.35	2.35	137	3.16	3.73	137	3.56	3.14	–	157	τRingIII(35), δCH_2(26), δCC(20)
94	3.88	0.88	91	2.80	0.66	90	3.03	0.49	–	97	τPhII(39), γCN(10), τRingIII(25)
55	0.01	0.05	66	0.01	0.39	65	0.01	0.16	–	63	τCN(79), τCH_2(10)
28	0.83	7.12	29	0.41	9.20	29	0.42	8.24	–	–	γRingIII(44), δCH_2(38)
24	0.34	7.81	21	0.09	10.03	22	0.14	7.88	–	–	τCH_2(78)
13	0.16	10.82	16	0.61	9.60	14	0.61	8.20	–	–	τCH_2(62)

[a] Abbreviations: υ-stretching; δ-in-plane deformation; γ-out-of-plane deformation; τ-twisting; as-asymmetric; s-symmetric.

is typically exhibited as a multiplicity of weak to moderate bands, compared with the aliphatic C—H stretch [38]. Klot and Collier [33] reported the bands at 3085, 3074, 3065 and 3045 cm^{-1} as υCH modes for benzoxazole. The bands observed at 3103, 3078, 3057 cm^{-1} in the IR and 3071, 3061 cm^{-1} in the Raman spectrum are assigned as the C—H stretching modes of the phenyl rings. The SDD calculations give these modes in the range 3083–3131 cm^{-1}.

The benzene ring possesses six ring stretching vibrations, of which the four with the highest wave numbers (occurring near 1600, 1580, 1490 and 1440 cm^{-1}) are good group vibrations. In the absence of ring conjugation, the band near 1580 cm^{-1} is usually weaker than that at 1600 cm^{-1}. The fifth ring stretching vibration which is active near 1335 ± 35 cm^{-1} a region which overlaps strongly with that of the CH in-plane deformation and the intensity is in general, low or medium high [22]. The sixth ring stretching vibration or ring breathing mode appears as a weak band near 1000 cm^{-1} in mono, 1,3-di and 1,3,5-trisubstituted benzenes. In the other wise substituted benzene, however, this vibration is substituent sensitive and difficult to distinguish from the ring in-plane deformation.

Since the identification of all the normal modes of vibrations of large molecules is not trivial, we tried to simplify the problem by considering each molecule as substituted benzene. Such an idea has already been successfully utilized by several workers for the vibrational assignments of molecules containing multiple homo- and hetero aromatic rings [37,39–42]. In the following discussion, the phenyl rings attached with ortho and para substitution are assigned as PhI and PhII, respectively and the benzoxazole ring as RingIII. The modes in the two phenyl rings will differ in wave number and the magnitude of splitting will depend on the strength of interactions between different parts (internal coordinates) of the two rings. For some modes, this splitting is so small that they may be considered as quasi-degenerate and for the other modes a significant amount of splitting is observed. Such observations have already been reported [30,37,39,43]. For the title compound, the bands observed at 1608, 1453, 1422, 1268 cm^{-1} in the IR and 1615, 1597, 1455, 1425, 1268 cm^{-1} in the Raman spectrum are assigned as υPhI modes with 1598, 1589, 1442, 1415, 1271 cm^{-1} as SDD values. For the title compound, PED analysis gives the ring breathing mode of PhI at 1081 cm^{-1} [44]. For the phenyl ring PhI, the bands observed at 1134, 1104, 1005 cm^{-1} in the IR spectrum and at 1149, 1107, 1005 cm^{-1} in the Raman spectrum are assigned as in-plane CH deformation modes. Also SDD calculations give these modes at 1149, 1141, 1108, 1003 cm^{-1} which are in agreement with literature [22].

For para substitued benzenes, the δCH modes are seen in the range 995–1315 cm^{-1} [22]. Bands observed at 1197, 1173 cm^{-1} in the IR spectrum and at 1199, 1175 cm^{-1} in the Raman spectrum are assigned as δCH modes for the ring PhII. The corresponding theoretical values (SDD) are 1309, 1181, 1170 and 1094 cm^{-1}. For the para substituted di-heavy phenyl ring, the ring stretching modes υPh modes are expected in the range 1280–1620 cm^{-1} [22]. In this case υPhII modes are assigned at 1585, 1576, 1468, 1372, 1343 cm^{-1} theoretically and observed at 1568, 1489, 1392, 1346 cm^{-1} in IR spectrum and at 1568, 1488, 1375, 1345 cm^{-1} in Raman spectrum. The ring breathing modes for the para di-substituted benzenes with entirely different substituents [45] have been reported to be strongly IR active with typical bands in the interval 740–840 cm^{-1}. For the title compound, this is confirmed by the strong band in the infrared spectrum at 744 cm^{-1} which finds support from the computational results that on 753 cm^{-1}. Ambujakshan et al. [12] reported a value 792 cm^{-1} (IR) and 782 cm^{-1} (HF) as ring breathing mode.

The C—H out-of-plane deformations are observed between 1000 and 700 cm^{-1} [22]. Generally the C—H out-of-plane deformations with the highest wave numbers have a weaker intensity than those absorbing at lower wave numbers. The out-of-plane γCH modes are observed at 913, 768 cm^{-1} in the IR spectrum, 961, 919, 862 cm^{-1} in the Raman spectrum for PhI and at 869 cm^{-1} in the IR spectrum for PhII. The corresponding SDD values are 985, 941, 862, 764 cm^{-1} for PhI and 992, 989, 868, 854 cm^{-1} for PhII. A very strong CH out-of plane deformation band, occurring at 840 ± 50 cm^{-1} is typical for 1,4-disubstituted benzenes [22]. For the title compound, a very strong γCH is observed at 869 cm^{-1} in IR spectrum. The SDD calculations give a γCH at 868 cm^{-1}. Again according to literature [22,34] a lower γCH absorbs in the neighborhood 820 ± 45 cm^{-1}, but is much weaker or infrared inactive and the corresponding theoretical mode is 854 cm^{-1}.

The benzoxazole ring stretching vibrations exist in the range 1504–1309 cm^{-1} in both spectra [30,46]. Bands observed at 1504, 1433, 1418 cm^{-1} in the Raman spectrum [30] and 1499, 1474, 1412 and 1309 cm^{-1} in the IR spectrum are assigned as the ring stretching vibrations. Klots and Collier [33] reported the bands at 1615, 1604, 1475 and 1451 cm^{-1} as fundamental ring vibrations of the benzoxazole ring. For benzoxazole, Klots and Collier [33] reported the bands at 932, 847 and 746 cm^{-1} as out-of-plane deformations for the benzene ring. According to Collier and Klots [47] the nonplanar vibrations are observed at 970, 932, 864, 847, 764, 620, 574, 417, 254, 218 cm^{-1} for benzoxazole and at 973, 939, 856, 757, 729, 584, 489, 419, 207, 192 cm^{-1} for benzothiazole. The planar modes below 1000 cm^{-1} for benzoxazole are reported to be at 920, 870, 778, 622, 538, 413 cm^{-1} and for benzothiazole at 873, 801, 712, 666, 531, 504, 530 cm^{-1} [47]. The planar and non-planar modes are also identified and assigned (Table 1).

4.2. Optimized geometry and first hyperpolarizability

To best of our knowledge, the XRD of the title compound is not yet reported. The optimized molecular structure of 2-(p-nitro benzyl)benzoxazole was determined by using Gaussian09 program. The optimized geometry is summarized as supporting material (Table S1). From Table S1, the C—C bond length of C_3—C_4 (1.4153 Å) is greater than that of C_4—C_5 (1.3939 Å) and C_2—C_3 (1.4036 Å), because of the delocalization of electron density of C_3—C_4 with the ring III. Also C_4—O_{10}, C_{12}—O_{10}, C_3—N_{11} and C_{12}—N_{11} bond lengths are different because of the difference in their environment, also assumes a double bond character in C_{12}—N_{11}. The bond angle between C_{13}—C_{12}—O_{10} (117.0°) and C_{13}—C_{12}—N_{11} (129.0°) indicates the π bond character of the former. The large difference between the bond lengths of C_{12}—C_{13} and C_{13}—C_{16} are because of the polarity difference of the attaching groups. The C—N bond length of C_3—N_{11} and C_{23}—N_{26} is only because of the greater delocalization in the nitro benzene entity.

Bond angles of C_5—C_4—O_{10} and C_2—C_3—N_{11} are higher than 120° indicates the presence of hyper conjugative interaction. The broadening of C_4—C_5—H_8 and C_3—C_2—H_7 bond angles than that of other C—C—H bond angles also indicates the delocalization of charge in the III ring. The reduced bond angles of C_{21}—C_{23}—N_{26}, C_{19}—C_{23}—N_{26} and H_{25}—C_{21}—C_{23}, H_{24}—C_{19}—C_{23} indicating the higher electronegative property of nitro group.

The substitution of nitro group in the phenyl ring increases the C—C bond lengths C_{21}—C_{23} and C_{23}—C_{19} of the benzene ring. Nitro group is highly electronegative and tries to obtain additional electron density of the benzene ring. It attempts to draw it from the neighboring atoms, which move closer together, in order to share the remaining electrons more easily. Due to this the bond angle *A*(21,23,19) is found to be 130.0° in the present calculation, which is 120° for normal benzene. Similarly, the bond lengths C_{21}—C_{23} and C_{23}—C_{19} are 1.4048 Å and 1.4069 Å, respectively, which is 1.3864 Å for benzene. For the title compound the bond lengths C_4—O_{10}, C_3—N_{11} are found to be 1.4081 and 1.4226 Å while for 2-mercaptobenzoxazole [48] these are, respectively, 1.3436 and 1.3739 Å. The bond lengths N_{11}—C_{12}, O_{10}—C_{12}, C_4—C_3 are found to increase to 1.3112, 1.4215 and 1.4153 Å from the values 1.3001, 1.3804 and 1.3927 Å obtained for 2-mercaptobenzoxazole [30]. These changes in bond lengths for the title compound can be attributed to the conjugation of the phenyl ring and the presence of a CH_2 group in the neighboring position.

The aromatic ring of the title compound is somewhat irregular and the spread of CC bond distance is 1.3939–1.4195 Å in PhI and 1.4013–1.4141 Å in PhII, which is similar to the spread reported by Smith et al. [49]. CH bond lengths in rings I and II of the title compound lie respectively between 1.0846–1.0868 Å and 1.0842–1.0870 Å. Chambers et al. [50] reported the N—O bond lengths in the range 1.2201–1.2441 Å and C—N bond length as 1.4544 Å. The experimental values of N—O bond lengths are 1.222–1.226 Å and C—N lengths in the range 1.442–1.460 Å [51]. Sundaraganesan et al. [52] reported C—N bond lengths as 1.453, 1.460 Å and N—O bond lengths in the range 1.2728–1.2748 Å. For the title compound, the C—N bond length is 1.4761 Å and N—O bond lengths are 1.2797, 1.2800 Å, which are in agreement with the reported values. The CNO angles are reported [52] in the range 117.4–118.7°, where as for the title compound it is 118.2°. Purkayastha and Chattopadhyay [53] reported N_{11}=C_{12}, N_{11}—C_3 bond lengths as 1.3270, 1.400 Å for benzothiazole and 1.3503, 1.407 Å for benzimidazole compounds. Ambujakshan et al. [12] has reported the same as 1.2753 and 1.3892 Å. In the present case, the respective bond lengths are 1.3112 and 1.4226 Å.

Lifshitz et al. [54] reported the bond lengths for N_{11}—C_{12}, O_{10}—C_{12}, O_{10}—C_4, C_3—C_2, C_4—C_5, C_3—C_4, and N_{11}—C_3 as 1.291, 1.372, 1.374, 1.39, 1.4, 1.403 and 1.401 Å. The corresponding values in the present case are 1.3112, 1.4215, 1.4081, 1.4036, 1.3939, 1.4153 and 1.4226 Å. Corresponding values are reported as 1.2753, 1.3492, 1.359, 1.3768, 1.3879, 1.3784, 1.3892 Å [12] and 1.2727, 1.347, 1.3594, 1.3884, 1.3777, 1.3776, 1.3903 Å [11]. The bond lengths C_4—O_{10}, C_3—N_{11}, N_{11}—C_{12}, C_{12}—O_{10} and C_3—C_4 are found to be 1.3436, 1.3739, 1.3001, 1.3804 and 1.3827 Å for mercaptobenzoxazole [35]. The bond angles of the NO_2 group of the title compound O_{28}—N_{26}—O_{27} = 123.7, O_{28}—N_{26}—C_{23} = 118.2, and O_{27}—N_{26}—C_{23} = 118.2 are in agreement with the values 123.5, 118.7, and 117.9° given by Saeed et al. [55].

The benzoxazole moiety is slightly tilted from ortho substituted phenyl ring as is evident from the torsion angles, C_6—C_5—C_4—O_{10} = 179.8, C_5—C_4—O_{10}—C_{12} = −179.8, C_1—C_2—C_3—N_{11} = −179.8 and C_2—C_3—N_{11}—C_{12} = 179.8° and methylene group is more tilted from the para substituted phenyl ring as is evident from torsion angles, C_{21}—C_{18}—C_{16}—C_{13} = −178.8, C_{18}—C_{16}—C_{13}—C_{12} = −124.0, C_{19}—C_{17}—C_{16}—C_{13} = 178.8 and C_{17}—C_{16}—C_{13}—C_{12} = 56.9°. The torsion angles C_{16}—C_{13}—C_{12}—N_{11} = −96.1 and C_{16}—C_{13}—C_{12}—O_{10} = 82.0°, which shows the COC and CON groups are in different planes.

The calculated first hyperpolarizability of the title compound is 10.7×10^{-30} esu, which comparable with the reported values of similar derivatives [56] and which is 82.31 times that of the standard NLO material urea (0.13×10^{-30} esu) [57]. We conclude that the title compound is an attractive object for future studies of nonlinear optical properties.

4.3. NBO Analysis

The natural bond orbitals (NBO) calculations were performed using NBO 3.1 program [58] as implemented in the Gaussian09 package at the DFT/B3LYP level in order to understand various second-order interactions between the filled orbitals of one subsystem and vacant orbitals of another subsystem, which is a measure of the intermolecular delocalization or hyper conjugation. NBO analysis provides the most accurate possible 'natural Lewis structure' picture of 'j' because all orbital details are mathematically chosen to include the highest possible percentage of the electron density. A useful aspect of the NBO method is that it gives information about interactions of both filled and virtual orbital spaces that could enhance the analysis of intra and inter molecular interactions.

The second-order Fock-matrix was carried out to evaluate the donor–acceptor interactions in the NBO basis. The interactions result in a loss of occupancy from the localized NBO of the idealized Lewis structure into an empty non-Lewis orbital. For each donor (i) and acceptor (j) the stabilization energy (*E*2) associated with the delocalization $i \rightarrow j$ is determined as:

$$E(2) = \Delta E_{ij} = q_i \frac{(F_{i,j})^2}{(E_j - E_i)}$$

q_i is the donor orbital occupancy; E_i, E_j the diagonal elements; F_{ij} is the off diagonal NBO Fock matrix element.

In NBO analysis large *E*(2) value shows the intensive interaction between electron-donors and electron-acceptors, and greater the extent of conjugation of the whole system, the possible intensive interaction are given as supporting material (Table S2). The second-order perturbation theory analysis of Fock-matrix in NBO basis shows strong intermolecular hyper conjugative interactions are formed by orbital overlap between n(O) and π*(N—O), π*(N—C) bond orbitals which result in ICT causing stabilization of the system. These interactions are observed as an increase in electron density (ED) in N—O and N—C anti bonding orbital that weakens the respective bonds. There occurs a strong inter molecular hyper conjugative interaction of N_{26}—O_{27} from O_{28} of $n_3(O_{28}) \rightarrow \pi^*(N_{26}$—$O_{27})$ which increases ED(0.66 e) that weakens the respective

bonds N_{26}—O_{27} (1.2649) leading to stabilization of 175.41 kJ/mol and also the hyper conjugative interaction of N_{11}—C_{12} from O_{10} of $n_2(O_{10}) \rightarrow \pi^*(N_{11}—C_{12})$ which increases ED(0.26 e) that weakens the respective bonds N_{11}—C_{12} (1.3048) leading to stabilization of 32.22 kJ/mol. These interactions are observed as an increase in electron density (ED) in N—O and N—C anti bonding orbitals that weakens the respective bonds.

The increased electron density at the oxygen atoms leads to the elongation of respective bond length and a lowering of the corresponding stretching wave number. The electron density (ED) is transferred from the n(O) to the anti-bonding π^* orbital of the N—O and N—C bonds, explaining both the elongation and the red shift [59]. The hyper conjugative interaction energy was deduced from the second-order perturbation approach. Delocalization of electron density between occupied Lewis-type (bond or lone pair) NBO orbitals and formally unoccupied (anti bond or Rydberg) non-Lewis NBO orbitals corresponds to a stabilizing donor–acceptor interaction. The C=N and NO_2 stretching modes can be used as a good probe for evaluating the bonding configuration around the N atoms and the electronic distribution of the benzene molecule. Hence the 2-(p-Nitro benzyl)benzoxazole structure is stabilized by these orbital interactions.

The NBO analysis also describes the bonding in terms of the natural hybrid orbital $n_2(O_{27})$, which occupy a higher energy orbital(−0.29907a.u.) with considerable p-character (99.76%) and low occupation number (1.90941) and the other $n_1(O_{27})$ occupy a lower energy orbital(—0.82007) with p-character (21.22%) and high occupation number (1.98353 a.u.). Thus, a very close to pure p-type lone pair orbital participates in the electron donation to the π^*(-N—O) orbital for $n2(O_{27}) \rightarrow \sigma^*$(N—O) interaction in the compound. The result is tabulated as supporting material (Table S3).

4.4. Mulliken charges

Mulliken charges are calculated by determining the electron population of each atom as defined in the basis functions. The charge distributions calculated by the Mulliken [60] and NBO methods for the equilibrium geometry of 2-(p-Nitro benzyl)benzoxazole are given as supporting material (Table S4). The charge distribution on the molecule has an important influence on the vibrational spectra. In 2-(p-nitro benzyl)benzoxazole, the Mulliken atomic charge of the carbon atoms in the neighborhood of C_{12}, C_4 and C_{23} become more positive, shows the direction of delocalization and shows that the natural atomic charges are more sensitive to the changes in the molecular structure than Mulliken's net charges. The results are represented as supporting material (Fig. S2).

Also we done a comparison of Mulliken charges obtained by different basic sets and tabulated it as supporting material (Table S5) in order to assess the sensitivity of the calculated charges to changes in (i) the choice of the basis set; (ii) the choice of the quantum mechanical method. The results can, however, better be represented in graphical form as shown as supporting material (Fig. S3). We have observed a change in the charge distribution by changing different basis sets.

4.5. Electronic absorption spectra

Electronic transitions are usually classified according to the orbitals engaged or to specific parts of the molecule involved. Common types of electronic transitions in organic compounds are π–π^*, n–π^* and π^*(acceptor)–π(donor). The UV–visible bands in 2-(p-Nitro benzyl) benzoxazole are observed at 279,273, and 208 nm. Observed band at 208 nm is due to the π–π^*. The moderatly intense band centered at 273 nm is due to the partly forbidden n–π^* transition from HOMO to LUMO. The more intense band observed at 279 nm belonged to the dipole-allowed π–π^* transition [61].

In order to understand the electronic transitions of 2-(p-nitro benzyl)benzoxazole, TD-DFT calculation on electronic absorption spectrum in vaccum was performed. TD-DFT calculation is capable of describing the spectral features of 2-(p-nitro benzyl)benzoxazole because of the qualitative agreement of line shape and relative strength as compared with experiment. The absorption spectra of organic compounds stem from the ground-to-excited state vibrational transition of electrons. The intense band in the UV range of the electronic absorption spectrum is observed at 208 nm, which is indicating the presence of chromophoric NO_2 in the ring. The calculated four lowest-energy transitions of the molecule from TD-DFT method and the observed electronic transitions are listed as supporting material (Table S6) [62]. From the table the calculated energy transitions are red shifted from the experimental value, because these bands are observed in gas phase with considering the effect of ethanol solvent.

The solvent effect on the absorption wavelengths and excitation energies are also examined by applying polarizable continuum model (PCM) TD-DFT method. The calculated absorption wavelengths, oscillator strengths, excitation energies of molecule in gas phase as well as in ethanol solvent medium are presented in Table S6 and theoretically simulated UV–Visible spectrum in ethanol solvent and experimental spectrum are given as supporting information (Fig. S1) for comparing their energetic behavior. In the electronic spectrum shows the strong intensity peak at the maximum absorption wavelength of 318 nm is caused by n–π transitions. The oscillator strength of this peak is 0.3459.

4.6. ^1H NMR spectrum

The experimental spectrum data of 2-(p-nitrobenzyl) benzoxazole in DMSO with TMS as internal standard is obtained at 400 MHz and is displayed as supporting material (Table S7). The absolute isotropic chemical shielding of 2-(p-nitrobenzyl) benzoxazole was calculated by B3LYP/GIAO model [63]. Relative chemical shifts were then estimated by using the corresponding TMS shielding: σ_{calc}.(TMS) calculated in advance at the same theoretical level as this paper. Numerical values of chemical shift $\delta_{calc} = \sigma_{calc}$.(TMS)–$\sigma_{calc}$ together with calculated values of σ_{calc}.(TMS), are reported as supporting material (Table S7). It could be seen from Table S7 that chemical shift was in agreement with the experimental ^1H NMR data. Thus, the results showed that the predicted proton chemical shifts were in good agreement with the experimental data for 2-(p-nitrobenzyl) benzoxazole.

4.7. PES scan studies

A detailed potential energy surface (PES) scan on dihedral angles N_{11}—C_{12}—C_{13}—C_{16}, C_{12}—C_{13}—C_{16}—C_{17} and C_{12}—C_{13}—C_{16}—C_{18} have been performed at B3LYP/6-31G(d) level to reveal all possible conformations of 2-(p-Nitrobenzyl)benzoxazole. The PES scan was carried out by minimizing the potential energy in all geometrical parameters by changing the torsion angle at every 10° for a 180° rotation around the bond. The results obtained in PES scan study by varying the torsion perturbation around the methyl bonds (CH_2) are plotted as supporting material (Figs. S4–S6). For the N_{11}—C_{12}—C_{13}—C_{16} rotation, the minimum energy was obtained at −98.8° in the potential energy curve of energy −874.59411 Hartrees. For the C_{12}—C_{13}—C_{16}—C_{17} rotation, the minimum energy occurs at 56.6° in the potential energy curve of energy −874.412211. It is found that on rotation of the ring structure, about the torsion angle C17—C16—C13—C12 the relative energy found to be minimum when the angle between the two rings are about 57.0°. For the C_{12}—C_{13}—C_{16}—C_{18} rotation, the minimum energy occur at

−124.4° in the potential energy curve of energy −874.33165 Hartrees.

4.8. Molecular electrostatic potential

MEP is related to the ED and is a very useful descriptor in understanding sites for electrophilic and nucleophilic reactions as well as hydrogen bonding interactions [64,65]. The electrostatic potential $V(r)$ is also well suited for analyzing processes based on the "recognition" of one molecule by another, as in drug-receptor, and enzyme-substrate interactions, because it is through their potentials that the two species first "see" each other [66,67]. To predict reactive sites of electrophilic and nucleophilic attacks for the investigated molecule, MEP at the B3LYP/6-31G(d,p) optimized geometry was calculated. The negative (red and yellow) regions of MEP were related to electrophilic reactivity and the positive (blue) regions to nucleophilic reactivity (Fig. S7). From the MEP it is evident that the negative charge covers the nitro group and the positive region is over the methyl group. The more electro negativity in the nitro group makes it the most reactive part in the molecule.

4.9. HOMO–LUMO band gap

HOMO and LUMO are the very important parameters for quantum chemistry. The conjugated molecules are characterized by a highest occupied molecular orbital–lowest unoccupied molecular orbital (HOMO–LUMO) separation, which is the result of a significant degree of ICT from the end-capping electron-donor groups to the efficient electron-acceptor groups through π-conjugated path. The strong charge transfer interaction through π-conjugated bridge results in substantial ground state donor–acceptor mixing and the appearance of a charge transfer band in the electronic absorption spectrum. Therefore, an ED transfer occurs from the more aromatic part of the π-conjugated system in the electron-donor side to its electron-withdrawing part. The atomic orbital components of the frontier molecular orbitals are shown as supporting material (Figs. S8 and S9). The HOMO–LUMO energy gap value is found to be 3.592 eV, which is responsible for the bioactive property of the compound 2-(p-Nitrobenzyl)benzoxazole, as reported in literature [68–70].

5. Conclusion

FT-IR and FT-Raman spectra of 2-(p-nitrobenzyl) benzoxazole were recorded and analyzed. The vibrational wavenumbers were computing at various levels of theory. The data obtained from theoretical calculations are used to assign vibrational bands obtained experimentally. The geometrical parameters of the title compound are in agreement with that of similar derivatives. The simultaneous activation of the phenyl ring stretching modes in IR and Raman spectra are evidence for charge transfer interaction between the donor and the acceptor group through the π system. This is responsible for the bioactivity of the molecule. The NBO analysis confirms the ICT formed by the orbital overlap between n(O) and σ^* (N—O). A very close to pure p-type lone pair orbital participates in the electron donation to the σ^*(C—C) orbital for $n2(O_{27}) \rightarrow \sigma^*$ (N—O) interaction in the molecule. Overall, the TD-DFT calculations on the molecule provided deep insight into their electronic structures and properties. In addition, the calculated ^{1}H NMR and UV–Vis results are all in good agreement with the experimental data. The lowering of HOMO–LUMO band gap supports bioactive property of the molecule. MEP predicts the most reactive part in the molecule. The calculated first hyperpolarizability is comparable with the reported values of similar derivatives and is an attractive object for future studies of nonlinear optics.

Acknowledgement

JBB is thankful to University of Kerala, India for a research fellowship and this work was carried out using the Turing HPC infrastructure at the CalcUA core facility of the Universiteit Antwerpen, a division of the Flemish Supercomputer Center VSC, funded by the Hercules Foundation, the Flemish Government (department EWI) and the Universiteit Antwerpen.

Appendix A. Supplementary material

Supplementary data associated with this article can be found, in the online version, at http://dx.doi.org/10.1016/j.molstruc.2013.04.044.

References

[1] W.A. Skinner, F. Gualtiere, G. Brody, A.H. Fieldsteel, J. Med. Chem. 14 (1971) 546.
[2] D.W. Dunwell, D. Evans, T.A. Hicks, C.H. Cashin, A. Kitchen, J. Med. Chem. 18 (1975) 53.
[3] K.H. Michel, L.D. Boeck, M.M. Hoehn, N.D. Jones, M.O. Chaney, J. Antibiot. 37 (1984) 441.
[4] W.D. Dunwell, D. Evans, J. Med. Chem. 20 (1977) 797.
[5] G. Wagner, B. Eppner, Pharmazie 35 (1980) 285.
[6] Farbenfabriken, A.G.Bayer, Netherlands Patent 6505511 (1965).
[7] I. Yalcin, E. Sener, S. Ozden, A. Akin, S. Yildiz, J. Pharm. Sci. 11 (1986) 257.
[8] E. Sener, S. Ozden, I. Yalcin, T. Ozden, A. Akin, S. Yildiz, J. Pharm. Sci. 11 (1986) 190.
[9] S. Ozden, T. Ozden, E. Sener, I. Yalcin, A. Akin, S. Yildiz, J. Pharm. Sci. 12 (1987) 39.
[10] E. Sener, I. Yalcin, S. Ozden, T. Ozden, A. Akin, S. Yildiz, J. Med. Pharm. 11 (1987) 391.
[11] P.L. Anto, C.Y. Panicker, H.T. Varghese, D. Philip, O. Temiz-Arpaci, B. Tekiner-Gulbas, I. Yildiz, Spectrochim. Acta Part A 67 (2007) 744.
[12] K.R. Ambujakshan, V.S. Madhavan, H.T. Varghese, C.Y. Panicker, O. Temiz-Arpaci, B. Tekiner-Gulbas, I. Yildiz, Spectrochim. Acta Part A 69 (2008) 782.
[13] E. Oksuzoglu, B. Tekiner-Gulbas, S. Alper, O. Temiz-Arpaci, T. Ertan, I. Yildiz, N. Diril, E. Sener-Aki, I. Yalcin, J. Enzyme Inhib, Med. Chem. 23 (2008) 37.
[14] I. Yalcin, E. Sener, T. Ozden, S. Ozden, A. Akin, Eur. J. Med. Chem. 25 (1990) 705.
[15] Gaussian 09, Revision B.01, M.J. Frisch, G.W. Trucks, H.B. Schlegel, G.E. Scuseria, M.A. Robb, J.R. Cheeseman, G. Scalmani, V. Barone, B. Mennucci, G.A. Petersson, H. Nakatsuji, M. Caricato, X. Li, H.P. Hratchian, A.F. Izmaylov, J. Bloino, G. Zheng, J.L. Sonnenberg, M. Hada, M. Ehara, K. Toyota, R. Fukuda, J. Hasegawa, M. Ishida, T. Nakajima, Y. Honda, O. Kitao, H. Nakai, T. Vreven, J.A. Montgomery, Jr., J.E. Peralta, F. Ogliaro, M. Bearpark, J.J. Heyd, E. Brothers, K.N. Kudin, V.N. Staroverov, T. Keith, R. Kobayashi, J. Normand, K. Raghavachari, A. Rendell, J.C. Burant, S.S. Iyengar, J. Tomasi, M. Cossi, N. Rega, J.M. Millam, M. Klene, J.E. Knox, J.B. Cross, V. Bakken, C. Adamo, J. Jaramillo, R. Gomperts, R.E. Stratmann, O. Yazyev, A.J. Austin, R. Cammi, C. Pomelli, J.W. Ochterski, R.L. Martin, K. Morokuma, V.G. Zakrzewski, G.A. Voth, P. Salvador, J.J. Dannenberg, S. Dapprich, A.D. Daniels, O. Farkas, J.B. Foresman, J.V. Ortiz, J. Cioslowski, D.J. Fox, Gaussian, Inc., Wallingford CT, 2010.
[16] J.B. Foresman, in: E. Frisch (Ed.), Exploring Chemistry with Electronic Structure Methods: A Guide to Using Gaussian, Gaussian, Inc., Pittsburg, PA, 1996.
[17] P.J. Hay, W.R. Wadt, J. Chem. Phys. 82 (1985) 270.
[18] J. Zhao, Y. Zhang, L. Zhu, J. Mol. Struct. Theochem. 671 (2004) 179.
[19] GaussView, Version 5, Roy Dennington, Todd Keith and John Millam, Semichem Inc., Shawnee Mission KS, 2009.
[20] J.M.L. Martin, C. Van Alsenoy, GAR2PED, A Program to Obtain a Potential Energy Distribution from a Gaussian Archive Record, University of Antwerp, Belgium, 2007.
[21] D.A. Kleinman, Phys. Rev. 126 (1962) 1977.
[22] N.P.G. Roeges, A Guide to the Complete Interpretation of Infrared Spectra of Organic Structures, Wiley, New York, 1994.
[23] R.M. Silverstein, F.X. Webster, Spectrometric Identification of Organic Compounds, sixth ed., John Wiley, Asia, 2003.
[24] A. Perjessy, D. Rasala, P. Tomasik, R. Gawinecki, Collect. Czech. Chem. Commun. 50 (1985) 2443.
[25] J.F. Brown Jr., J. Am. Chem. Soc. 77 (1955) 6341.
[26] J.H.S. Green, W. Kynaston, A.S. Lindsey, Spectrochim. Acta 17 (1961) 486.
[27] O. Exner, S. Kovac, E. Solcaniova, Collect. Czech. Chem. Commun. 37 (1972) 2156.
[28] G. Varsanyi, E. Molnar-Paal, K. Kosa, G. Keresztury, Acta Chim. Acad. Sci. Hung. 100 (1979) 481.
[29] V. Suryanarayana, A.P. Kumar, G.R. Rao, G.C. Panday, Spectrochim. Acta 48A (1992) 1481.
[30] R. Saxena, L.D. Kandpal, G.N. Mathur, J. Polym. Sci. Part A: Polym. Chem. 40 (2002) 3959.
[31] R.M. Silverstein, G.C. Bassler, T.C. Morril, Spectrometric Identification of Organic Compounds, Fifth ed., John Wiley and Sons Inc., Singapore, 1991.

[32] K. Nakamoto, Infrared and Raman Spectrum of Inorganic and coordination Compounds, fifth ed., John Wiley and Sons, Inc., New York, 1997.
[33] T.D. Klots, W.B. Collier, Spectrochim. Acta 51A (1995) 1291.
[34] N.B. Colthup, L.H. Daly, S.E. Wiberly, Introduction to Infrared and Raman Spectroscopy, third ed., Academic Press, Boston, 1990.
[35] A. Bigotto, B. Pergolese, J. Raman Spectrosc. 32 (2001) 953.
[36] N. Sandhyarani, G. Skanth, S. Berchmanns, V. Yegnaraman, T. Pradeep, J. Colloid Interface Sci. 209 (1999) 154.
[37] P. Sett, N. Paul, S. Chattopadhyay, P.K. Mallick, J. Raman Spectrosc. 30 (1999) 277.
[38] J. Coates, in: R.A. Meyers (Ed.), Encyclopedia of Analytical Chemistry; Interpretation of Infrared Spectra, A Practical Approach, John Wiley and Sons Ltd., Chichester, 2000.
[39] P. Sett, S. Chattopadhyay, P.K. Mallick, Spectrochim. Acta 56A (2000) 855.
[40] P. Sett, S. Chattopadhyay, P.K. Mallick, J. Raman Spectrosc. 31 (2000) 177.
[41] V. Volovsek, G. Baranovic, L. Colombo, J.R. Durig, J. Raman Spectrosc. 22 (1991) 35.
[42] M. Muniz-Miranda, E. Castellucci, N. Neto, G. Sbrana, Spectrochim. Acta 39A (1983) 107.
[43] J.H.S. Green, Spectrochim. Acta 24 (1968) 1627.
[44] C.Y. Panicker, H.T. Varghese, K.R. Ambujakshan, S. Mathew, S. Ganguli, A.K. Nanda, C. Van Alsenoy, Y.S. Mary, J. Mol. Struct. 963 (2010) 137.
[45] G. Varsanyi, Assignments of Vibrational Spectra of Seven Hundred Benzene Derivatives, Wiley, New York, 1974.
[46] W.K. Yi, C.W. Park, M.S. Kim, K. Kim, Bull. Korean Chem. Soc. 8 (1987) 291.
[47] W.B. Collier, T.D. Klots, Spectrochim. Acta 51A (1995) 1255.
[48] D.F. Eaton, Science 25 (1991) 281.
[49] G. Smith, D.E. Lynch, K.A. Byriel, C.H.L. Kennard, Aust. J. Chem. 48 (1995) 1133.
[50] R.D. Chambers, M.A. Fox, G. Sandford, J. Trmcic, A. Goeta, J. Fluorine Chem. 128 (2007) 29.
[51] N. Okabe, T. Nakamura, H. Fukuda, Acta Cryst. C49 (1993) 1678.
[52] N. Sundaraganesan, S. Ayyappan, H. Umamaheswari, B.D. Joshua, Spectrochim. Acta 66A (2007) 17.
[53] P. Purkayastha, N. Chattopadhyay, Phys. Chem. Chem. Phys. 2 (2000) 203.
[54] A. Lifshitz, C. Tamburu, A. Suslensky, F. Dubnikova, J. Phys. Chem. A 110 (2006) 4607.
[55] A. Saeed, S. Hussain, U. Florke, Turk. J. Chem. 32 (2008) 481.
[56] L.N. Kuleshova, M.Y. Antipin, V.N. Khrustalev, D.V. Gusev, G.V. Grintselev-Knyazev, E.S. Bobrikova, Cryst. Reports 48 (2003) 594.
[57] M. Adant, M. Dupuis, J.L. Bredas, Int. J. Quantum. Chem. 56 (1995) 497.
[58] E.D. Glendening, A.E. Reed, J.E. Carpenter, F. Weinhold, NBO Version 3.1.
[59] J. Choo, S. Kim, H. Joo, Y. Kwon, J. Mol. Struct. (Theochem.) 587 (2002) 1.
[60] R.S. Mulliken, J. Chem. Phys. 23 (1955) 1833.
[61] A. Varlan, M. Hillebran, J. Mol. Struct. 1036 (2013) 341.
[62] R.A. Ando, R.L.O.R. Cunha, L. Juliano, A.C. Boring, J. Raman Spectrosc. 39 (2008) 453.
[63] K. Wolinski, J.F. Hinton, P. Pulay, J. Am. Chem. Soc. 112 (1990) 8251.
[64] E. Scrocco, J. Tomasi, Adv. Quantum. Chem. 103 (1978) 115.
[65] F.J. Luque, J.M. Lopez, M. Orozco, Theor. Chem. Acc. 103 (2000) 343.
[66] P. Politzer, J.S. Murray, in: D.L.Beveridge, R. Lavery (Eds.), Theoretical Biochemistry and Molecular Biophysics: A Comprehensive Survey, vol. 2, ProteinAdenine Press, Schenectady, NY, 1991 (Chapter 13).
[67] E. Scrocco, J. Tomasi, Top. Curr. Chem. 42 (1973) 95.
[68] Y. Li, Y. Liu, H. Wang, X. Xiong, P. Wei, F. Li, Molecules 18 (2013) 877.
[69] H. Marouani, N. Raouafi, S. Toumi Akriche, S.S. Al-Deyab, M. Rzaigu, E-Journal Chem. 9 (2012) 772.
[70] B.A. Saeed, R.S. Elias, Sadiq M.-H. Ismael, K.A. Hussain, Am. J. Appl. Sci. 8 (2011) 773.